No return to reflection symmetry in freely decaying homogeneous turbulence

Katsunori Yoshimatsu*
Institute of Materials and Systems for Sustainability, Nagoya University, Nagoya 464-8601, Japan

Yukio Kaneda
Aichi Institute of Technology, 1247 Yachikusa, Yakusacho, Toyota 470-0392, Japan

(Received 8 September 2018; published 27 February 2019)

We consider the large-scale structure of freely decaying incompressible homogeneous anisotropic helical turbulence, whose energy spectrum $E(k)$ is given by $E(k) = Ck^2 + o(k^2)$ at $k \to 0$. Here $k = |\boldsymbol{k}|$, $\boldsymbol{k}$ is the wave vector, and C is a dynamical invariant. The helicity spectrum $H(k)$ is given by $H(k) = C_h k^3 + o(k^3)$ at $k \to 0$, where C_h is in general nonzero in helical turbulence. By generalizing Saffman's argument for nonhelical turbulence [Saffman, J. Fluid Mech. **27**, 581 (1967)] to helical turbulence, it is shown that C_h is another dynamical invariant. We present a theoretical analysis based on the time independence of the $O(k^0)$ term of the velocity correlation spectral tensor at $\boldsymbol{k} \to \boldsymbol{0}$ and a self-similarity assumption of flow evolution at large scales including the energy containing range scales. The analysis suggests that if the $O(k^0)$ term is reflection asymmetric at an initial instant, the turbulence does not relax to any reflection symmetric state at the large scales. A simple dimensional analysis yields the decay rates of the helicity and kinetic energy in the fully developed turbulence state. The theoretical results agree with results obtained by direct numerical simulation of incompressible helical turbulence in a periodic box.

DOI: 10.1103/PhysRevFluids.4.024611

I. INTRODUCTION

Saffman [1] considered the large-scale structure of freely decaying incompressible homogeneous turbulence where the velocity correlation spectral tensor $\hat{R}_{ij}(\boldsymbol{k})$, at an initial instant $t = t_0$, is given by

$$\hat{R}_{ij}(\boldsymbol{k}) = P_{i\alpha}P_{j\beta}M_{\alpha\beta} + o(1) \quad \text{at } \boldsymbol{k} \to \boldsymbol{0}. \tag{1}$$

Here $P_{ij} = \delta_{ij} - k_i k_j/k^2$, $\boldsymbol{k} = (k_1, k_2, k_3)$ is the wave vector, $k = |\boldsymbol{k}|$, $M_{\alpha\beta}$ is a $\boldsymbol{k}$-independent constant, δ_{ij} is Kronecker's delta, and the summation convention is used for repeated Greek subscripts. The tensor $\hat{R}_{ij}(\boldsymbol{k})$ is given by the Fourier transform of the second-order two-point velocity correlation tensor $R_{ij}(\boldsymbol{r}) = \langle u_i(\boldsymbol{x})u_j(\boldsymbol{x}+\boldsymbol{r})\rangle$, where a circumflex denotes the Fourier transform, $\boldsymbol{u}(\boldsymbol{x})$ is the velocity, $\langle\cdots\rangle$ denotes the ensemble average, $\boldsymbol{x}$ is the position, and $\boldsymbol{r}$ is the separation vector. Equation (1) implies that the energy spectrum defined by $E(k) = \frac{1}{2}\int |\hat{\boldsymbol{u}}(\boldsymbol{q})|^2 dS_k$ is given by

$$E(k) = Ck^2 + o(k^2) \quad \text{at } k \to 0, \tag{2}$$

where $\int \cdots dS_k$ denotes the integral of $\cdots$ over the spherical surface with the radius $|\boldsymbol{q}| = k$ and center at $\boldsymbol{q} = \boldsymbol{0}$. The $O(k^0)$ term in Eq. (1) has reflection symmetry, i.e., mirror symmetry. Saffman

*yoshimatsu@nagoya-u.jp

showed that this term is time independent so that $\hat{R}_{ij}(\boldsymbol{k})$ and $E(k)$ keep Eqs. (1) and (2), respectively, at any time t ($\geqslant t_0$). This implies that $M_{\alpha\beta}$ and C are time independent. This kind of turbulence with Eq. (1) is called here Saffman turbulence. The decay rate of the kinetic energy and the growth rate of an integral length scale for fully developed Saffman turbulence were derived by the use of the time independence and a self-similarity assumption [2].

Recently Saffman's argument has been generalized to include turbulence with the velocity correlation tensor where the leading order term is $O(k^0)$, as in Eq. (1); however, this term may have arbitrary dependence on the direction vector $\boldsymbol{k}/k$ and may not be limited to the form of Eq. (1) [3]. The energy spectrum keeps Eq. (2) at any time t ($\geqslant t_0$). Here we call this kind of turbulence generalized Saffman turbulence. The generalization showed that there are an infinite number of invariants, not limited to Saffman's invariants $M_{\alpha\beta}$. The large-scale structure need not have reflection symmetry. A self-similarity assumption of flow evolution at large scales including the energy containing range scales suggests that anisotropy in the large-scale statistics of generalized Saffman turbulence is persistent, i.e., the statistics do not return to isotropy, if $\hat{R}_{ij}(\boldsymbol{k})$ is anisotropic at $\boldsymbol{k} \to \boldsymbol{0}$ and $t = t_0$. For axisymmetric Saffman turbulence, this persistence of large-scale anisotropy is consistent with dimensional analysis and direct numerical simulation (DNS) [4] and large-eddy simulation [5]. The persistence was observed also in eddy-damped quasinormal Markovian (EDQNM) simulations [6,7]. Note that it is widely accepted that the statistics at sufficiently small scales in sufficiently high Reynolds number turbulence are homogeneous and isotropic. The persistence provides a counterexample of the traditional view, a return to isotropy even in the energy containing range for freely decaying homogeneous turbulence.

We then pose the following question: Do fully developed generalized Saffman turbulence statistics remain reflection asymmetric at large scales including the energy containing range scales, if $\hat{R}_{ij}(\boldsymbol{k})$ is reflection asymmetric at $\boldsymbol{k} \to \boldsymbol{0}$ and at $t = t_0$? We consider here reflection asymmetry due to the existence of the helicity defined by $\langle \boldsymbol{u} \cdot \boldsymbol{\omega} \rangle/2$, where $\boldsymbol{\omega}$ is the vorticity. The helicity, which is conserved for inviscid flow, is a typical statistical quantity characterizing reflection asymmetry and a measure of topological properties such as the degree of knottedness of vorticity (see, e.g., [8,9]). Kit *et al.* [10] pioneered the direct measurement of helicity density in laboratory experiments of turbulence. In DNSs [11,12], numerical simulation using hyperviscosity [13], and EDQNM simulations [14] of helical turbulent flows, the helicity spectrum $H(k)$, defined as $H(k) = \frac{1}{2} \int \hat{\boldsymbol{u}}(-\boldsymbol{q}) \cdot \hat{\boldsymbol{\omega}}(\boldsymbol{q}) dS_k$, and the energy spectrum $E(k)$ scale like $k^{-5/3}$ in the inertial subrange. This is in accordance with the prediction in Ref. [15] in the case of simultaneous energy and helicity cascades. Small-scale reflection asymmetry of the helical flows becomes weaker and the small-scale fields approach reflection symmetric states as scales becomes smaller [12–14].

The helicity spectrum satisfies $|H(k)| \leqslant kE(k)$ [16]. This inequality gives

$$H(k) = C_h k^3 + o(k^3) \quad \text{at } k \to 0 \tag{3}$$

if $E(k)$ is given by Eq. (2), where C_h is not sign definite. We call here incompressible homogeneous turbulence whose energy and helicity spectra are given by Eqs. (2) and (3), where $C \neq 0$ and $C_h \neq 0$ as helical Saffman turbulence. Equation (1) implies $C_h = 0$, i.e., $H(k) = o(k^3)$. However, the leading $O(k^0)$ term of $\hat{R}_{ij}(\boldsymbol{k})$ at $\boldsymbol{k} \to \boldsymbol{0}$ for generalized Saffman turbulence allows the k^3 helicity spectrum. Briard and Gomez [17] predicted the decay rates of kinetic energy and helicity in fully developed homogeneous isotropic helical Saffman turbulence, by using an EDQNM closure and dimensional analysis based on the analysis by Comte-Bellot and Corrsin [18]. The prediction implies that the kinetic energy decay rate is the same as the rate predicted by Ref. [2], and the helicity decays more rapidly than kinetic energy. The helicity decay rate different from the prediction was obtained in Ref. [19], which used the invariance of Saffman's integral and the invariance of an integral based on the helicity correlation. A discussion about the different helicity decay rates was given in Ref. [17], which stressed the importance of the inequality $|H(k)| \leqslant kE(k)$.

This paper is organized as follows. In Sec. II we present the theory [3] for the time independence of the $O(k^0)$ term of $\hat{R}_{ij}(\boldsymbol{k})$ at $\boldsymbol{k} \to \boldsymbol{0}$, by using the so-called $\mathcal{E}$-$\mathcal{Z}$-$\mathcal{H}$ decomposition exploited by

Cambon and Jacquin [20]. This decomposition well characterizes the antireflection symmetric part of $\hat{R}_{ij}(\boldsymbol{k})$. Using quantities based on $\mathcal{E}(\boldsymbol{k})$ and $\mathcal{H}(\boldsymbol{k})$, we will introduce a quantity to characterize the degree of reflection asymmetry in the energy containing range. It is shown that C_h is a dynamical invariant. Then, by using the time independence and a self-similarity assumption of large-scale flow evolution, it will be shown that large-scale reflection asymmetry due to helicity is persistent in fully developed anisotropic helical Saffman turbulence. Decay laws are derived by the use of a simple dimensional analysis. In Sec. III these theoretical results and the large-scale self-similarity are examined by DNS of incompressible helical turbulence in a periodic box. A summary is given in Sec. IV.

II. HELICAL SAFFMAN TURBULENCE

A. Helical mode decomposition and statistics of helical turbulence

We consider the freely decaying motion of an incompressible fluid whose density and kinematic viscosity are denoted by ρ and ν, respectively. The velocity field $\boldsymbol{u}(\boldsymbol{x}, t)$ is governed by the Navier-Stokes equation

$$\frac{\partial \boldsymbol{u}}{\partial t} + (\boldsymbol{u}\cdot\nabla)\boldsymbol{u} = -\frac{1}{\rho}\nabla p + \nu\nabla^2\boldsymbol{u} \tag{4}$$

and the divergence-free condition $\nabla\cdot\boldsymbol{u} = 0$, where $p(\boldsymbol{x}, t)$ is the pressure and $\nabla = (\partial/\partial x_1, \partial/\partial x_2, \partial/\partial x_3)$. Arguments such as $\boldsymbol{x}$ and t are omitted at will.

Let us define the Fourier transform of $\boldsymbol{u}$ by $\hat{\boldsymbol{u}}(\boldsymbol{k}, t) = (2\pi)^{-3}\int_{\mathbb{R}^3}\boldsymbol{u}(\boldsymbol{x}, t)\exp(-i\boldsymbol{k}\cdot\boldsymbol{x})d\boldsymbol{x}$. Then $\hat{\boldsymbol{u}}(\boldsymbol{k}, t)$ may be decomposed into two fields $\hat{\boldsymbol{u}}^{\pm}(\boldsymbol{k}, t)$, such as

$$\hat{\boldsymbol{u}}(\boldsymbol{k}, t) = \hat{\boldsymbol{u}}^{+}(\boldsymbol{k}, t) + \hat{\boldsymbol{u}}^{-}(\boldsymbol{k}, t), \quad \hat{\boldsymbol{u}}^{\pm}(\boldsymbol{k}, t) = \xi^{\pm}(\boldsymbol{k}, t)\boldsymbol{N}(\pm\tilde{\boldsymbol{k}}), \tag{5}$$

in $\boldsymbol{k}$ space, by the use of the helical mode $\boldsymbol{N}(\tilde{\boldsymbol{k}})$ [20], where $\tilde{\boldsymbol{k}} = \boldsymbol{k}/k$ and the double signs in $\hat{\boldsymbol{u}}^{\pm}(\boldsymbol{k}, t)$ correspond to the double signs in $\xi^{\pm}(\boldsymbol{k}, t)$ and $\boldsymbol{N}(\pm\tilde{\boldsymbol{k}})$. The mode $\boldsymbol{N}(\tilde{\boldsymbol{k}})$ is defined by

$$\boldsymbol{N}(\tilde{\boldsymbol{k}}) = \boldsymbol{e}^{(2)}(\tilde{\boldsymbol{k}}) - i\boldsymbol{e}^{(1)}(\tilde{\boldsymbol{k}}), \tag{6}$$

where $\boldsymbol{e}^{(1)}$ and $\boldsymbol{e}^{(2)}$ are the solenoidal unit vectors of the Craya-Herring basis,

$$\boldsymbol{e}^{(1)} = \frac{\tilde{\boldsymbol{k}}\times\boldsymbol{i}_3}{|\tilde{\boldsymbol{k}}\times\boldsymbol{i}_3|}, \quad \boldsymbol{e}^{(2)} = \frac{\tilde{\boldsymbol{k}}\times\boldsymbol{e}^{(1)}}{|\tilde{\boldsymbol{k}}\times\boldsymbol{e}^{(1)}|}, \tag{7}$$

in which $\boldsymbol{i}_3$ is taken as $\boldsymbol{i}_3 = (0, 0, 1)$. Here $\boldsymbol{e}^{(1)}(\tilde{\boldsymbol{k}})$, $\boldsymbol{e}^{(2)}(\tilde{\boldsymbol{k}})$, and $\boldsymbol{N}(\tilde{\boldsymbol{k}})$ satisfy $\boldsymbol{e}^{(1)}(-\tilde{\boldsymbol{k}}) = -\boldsymbol{e}^{(1)}(\tilde{\boldsymbol{k}})$, $\boldsymbol{e}^{(2)}(-\tilde{\boldsymbol{k}}) = \boldsymbol{e}^{(2)}(\tilde{\boldsymbol{k}})$, $|\boldsymbol{N}| = 2^{1/2}$, $\boldsymbol{N}(-\tilde{\boldsymbol{k}}) = \boldsymbol{N}^*(\tilde{\boldsymbol{k}})$, and $i\boldsymbol{k}\times\boldsymbol{N} = k\boldsymbol{N}$, where an asterisk denotes the complex conjugate. Readers interested in the helical mode and the decomposition are referred to Ref. [21].

The velocity correlation spectral tensor $\hat{R}_{ij}(\boldsymbol{k})$ satisfies $\langle\hat{u}_i(\boldsymbol{k}')\hat{u}_j(\boldsymbol{k})\rangle = \hat{R}_{ij}(\boldsymbol{k})\delta(\boldsymbol{k}+\boldsymbol{k}')$. We define the spectral correlation tensors of $\hat{u}_i^{\pm}(\boldsymbol{k})$, which are denoted by $\hat{R}_{ij}^{\pm}(\boldsymbol{k})$, as $\langle\hat{u}_i^{\pm}(\boldsymbol{k}')\hat{u}_j^{\pm}(\boldsymbol{k})\rangle = \hat{R}_{ij}^{\pm}(\boldsymbol{k})\delta(\boldsymbol{k}+\boldsymbol{k}')$. Then $\hat{R}_{\alpha\alpha}(\boldsymbol{k}) = \hat{R}_{\alpha\alpha}^{+}(\boldsymbol{k}) + \hat{R}_{\alpha\alpha}^{-}(\boldsymbol{k})$.

Let $\mathcal{E}(\boldsymbol{k})$ and $\mathcal{H}(\boldsymbol{k})$ be defined, respectively, by

$$\mathcal{E}(\boldsymbol{k}) = \tfrac{1}{2}\{\hat{R}_{\alpha\alpha}^{+}(\boldsymbol{k}) + \hat{R}_{\alpha\alpha}^{-}(\boldsymbol{k})\}, \quad \mathcal{H}(\boldsymbol{k}) = \tfrac{1}{2}\{\hat{R}_{\alpha\alpha}^{+}(\boldsymbol{k}) - \hat{R}_{\alpha\alpha}^{-}(\boldsymbol{k})\}. \tag{8}$$

The velocity-vorticity spectral correlation $\langle\hat{\boldsymbol{u}}(\boldsymbol{k}')\cdot\hat{\boldsymbol{\omega}}(\boldsymbol{k})\rangle$ is given by $2k\mathcal{H}(\boldsymbol{k})\delta(\boldsymbol{k}+\boldsymbol{k}')$, because $\hat{\boldsymbol{\omega}}(\boldsymbol{k}) = k\{\hat{\boldsymbol{u}}^{+}(\boldsymbol{k}) - \hat{\boldsymbol{u}}^{-}(\boldsymbol{k})\}$. Applying the Fourier transform to the second-order two-point velocity-vorticity correlation $\langle\boldsymbol{u}(\boldsymbol{x})\cdot\boldsymbol{\omega}(\boldsymbol{x}+\boldsymbol{r})\rangle$ that was introduced in Ref. [22], one obtains

$$k\mathcal{H}(\boldsymbol{k}) = \frac{1}{2(2\pi)^3}\int_{\mathbb{R}^3}\langle\boldsymbol{u}(\boldsymbol{x})\cdot\boldsymbol{\omega}(\boldsymbol{x}+\boldsymbol{r})\rangle\exp(-i\boldsymbol{k}\cdot\boldsymbol{r})d\boldsymbol{r} \tag{9}$$

(see e.g., [17]). The fields $\hat{\boldsymbol{u}}^{+}(\boldsymbol{k})$ and $\hat{\boldsymbol{u}}^{-}(\boldsymbol{k})$ have non-negative helicity $(k/2)|\hat{\boldsymbol{u}}^{+}(\boldsymbol{k})|^2$ and nonpositive helicity $-(k/2)|\hat{\boldsymbol{u}}^{-}(\boldsymbol{k})|^2$, respectively, since $\hat{\boldsymbol{u}}^{\pm}(-\boldsymbol{k})\cdot\hat{\boldsymbol{\omega}}^{\pm}(\boldsymbol{k}) = \pm k|\hat{\boldsymbol{u}}^{\pm}(\boldsymbol{k})|^2$.

The energy spectrum $E(k)$ and helicity spectrum $H(k)$ are written as

$$E(k) = \int \mathcal{E}(\boldsymbol{q}) dS_k, \quad H(k) = k \int \mathcal{H}(\boldsymbol{q}) dS_k, \tag{10}$$

where $\int \cdots dS_k$ denotes the integral of $\cdots$ over the spherical surface with the radius $|\boldsymbol{q}| = k$ and center at $\boldsymbol{q} = \boldsymbol{0}$. The fields $\boldsymbol{u}^{\pm}(\boldsymbol{x})$ were used to examine the roles of $\boldsymbol{u}^{\pm}$ in the energy and helicity fluxes [23,24]. Note that $\langle |\boldsymbol{u}|^2 \rangle = \langle |\boldsymbol{u}^+|^2 \rangle + \langle |\boldsymbol{u}^-|^2 \rangle$ and $\langle \boldsymbol{u}^+ \cdot \boldsymbol{u}^- \rangle = 0$.

Equation (8) gives $\langle |\boldsymbol{u}|^2 \rangle/2$ and $(\langle |\boldsymbol{u}^+|^2 \rangle - \langle |\boldsymbol{u}^-|^2 \rangle)/2$ as

$$\frac{\langle |\boldsymbol{u}|^2 \rangle}{2} = \int_{\mathbb{R}^3} \mathcal{E}(\boldsymbol{k}) d\boldsymbol{k}, \quad \frac{\langle |\boldsymbol{u}^+|^2 \rangle - \langle |\boldsymbol{u}^-|^2 \rangle}{2} = \int_{\mathbb{R}^3} \mathcal{H}(\boldsymbol{k}) d\boldsymbol{k}. \tag{11}$$

Because of Eq. (9), the total helicity $\langle \boldsymbol{u} \cdot \boldsymbol{\omega} \rangle/2$ is given by

$$\frac{1}{2} \langle \boldsymbol{u} \cdot \boldsymbol{\omega} \rangle = \int_{\mathbb{R}^3} k \mathcal{H}(\boldsymbol{k}) d\boldsymbol{k}. \tag{12}$$

The difference $\hat{R}^+_{\alpha\alpha}(\boldsymbol{k}) - \hat{R}^-_{\alpha\alpha}(\boldsymbol{k})$ or $\mathcal{H}(\boldsymbol{k})$ expresses the degree of reflection asymmetry due to helicity. The degree of the reflection asymmetry due to helicity can be characterized by the relative helicity $\langle \boldsymbol{u} \cdot \boldsymbol{\omega} \rangle / \sqrt{\langle |\boldsymbol{u}|^2 \rangle \langle |\boldsymbol{\omega}|^2 \rangle}$, where $\langle |\boldsymbol{\omega}|^2 \rangle$ in the denominator is a representative quantity in the dissipation range. We use here a quantity defined by

$$\frac{\langle |\boldsymbol{u}^+|^2 \rangle - \langle |\boldsymbol{u}^-|^2 \rangle}{\langle |\boldsymbol{u}|^2 \rangle} \tag{13}$$

to characterize the degree of the asymmetry in the energy containing range by using $\langle |\boldsymbol{u}^{\pm}|^2 \rangle$ that are representative quantities in the energy containing range like $\langle |\boldsymbol{u}|^2 \rangle$. The quantity (13) is zero if turbulence has reflection symmetry, i.e., $\langle |\boldsymbol{u}^+|^2 \rangle = \langle |\boldsymbol{u}^-|^2 \rangle$. The absolute value of (13) satisfies

$$\frac{|\langle |\boldsymbol{u}^+|^2 \rangle - \langle |\boldsymbol{u}^-|^2 \rangle|}{\langle |\boldsymbol{u}|^2 \rangle} \leqslant 1. \tag{14}$$

B. Velocity correlation spectral tensor

The velocity correlation spectral tensor $\hat{R}_{ij}(\boldsymbol{k}, t)$ may be written as

$$\hat{R}_{ij}(\boldsymbol{k}, t) = \mathcal{E}(\boldsymbol{k}, t) P_{ij} + \mathrm{Re}[\mathcal{Z}(\boldsymbol{k}, t) N_i(\tilde{\boldsymbol{k}}) N_j(\tilde{\boldsymbol{k}})] + i \mathcal{H}(\boldsymbol{k}, t) \epsilon_{ij\alpha} \tilde{k}_\alpha, \tag{15}$$

where $P_{ij} = \delta_{ij} - \tilde{k}_i \tilde{k}_j$, $\epsilon_{ij\alpha}$ is the alternating third-order tensor, and $\mathcal{Z}(\boldsymbol{k})$ is complex with $\mathcal{Z}(-\boldsymbol{k}) = \mathcal{Z}^*(\boldsymbol{k})$ [20,21]. Then Eqs. (5) and (15) give

$$\hat{R}^{\pm}_{ij}(\boldsymbol{k}) = \tfrac{1}{2} \{ \mathcal{E}(\boldsymbol{k}) \pm \mathcal{H}(\boldsymbol{k}) \} N_i(-\tilde{\boldsymbol{k}}) N_j(\tilde{\boldsymbol{k}}). \tag{16}$$

For generalized Saffman turbulence, it was shown that

$$\hat{R}_{ij}(\boldsymbol{k}) = \mathcal{E}_0(\tilde{\boldsymbol{k}}) P_{ij} + \mathrm{Re}[\mathcal{Z}_0(\tilde{\boldsymbol{k}}) N_i(\tilde{\boldsymbol{k}}) N_j(\tilde{\boldsymbol{k}})] + i \mathcal{H}_0(\tilde{\boldsymbol{k}}) \epsilon_{ij\alpha} \tilde{k}_\alpha + o(1) \tag{17}$$

at $\boldsymbol{k} \to \boldsymbol{0}$, where $\mathcal{E}_0(\tilde{\boldsymbol{k}}) \neq 0$ at an initial time $t = t_0$, and $\mathcal{E}_0(\tilde{\boldsymbol{k}})$, $\mathcal{Z}_0(\tilde{\boldsymbol{k}})$, and $\mathcal{H}_0(\tilde{\boldsymbol{k}})$ are $O(k^0)$ and depend on $\boldsymbol{k}$ only through the direction $\tilde{\boldsymbol{k}}$ [3]. From Eq. (17) we obtain

$$\hat{R}^{\pm}_{ij}(\boldsymbol{k}) = \tfrac{1}{2} \{ \mathcal{E}_0(\tilde{\boldsymbol{k}}) \pm \mathcal{H}_0(\tilde{\boldsymbol{k}}) \} N_i(-\tilde{\boldsymbol{k}}) N_j(\tilde{\boldsymbol{k}}) + o(1). \tag{18}$$

Similar to $\hat{R}_{ij}$ given by Eq. (1), $\hat{R}_{ij}$ given by Eq. (17) is also discontinuous at $\boldsymbol{k} = \boldsymbol{0}$. Equation (17) is not reflection symmetric in general, whereas Eq. (1) is reflection symmetric. Saffman [1] obtained Eq. (1) under the conditions that, at an initial instant $t = t_0$, the vorticity spectral correlation tensor $(2\pi)^{-3} \int_{\mathbb{R}^3} \langle \omega_i(\boldsymbol{x}) \omega_j(\boldsymbol{x} + \boldsymbol{r}) \rangle \exp(-i\boldsymbol{k} \cdot \boldsymbol{r}) d\boldsymbol{r}$ is reflection symmetric and is analytic in $\boldsymbol{k}$ at $\boldsymbol{k} = \boldsymbol{0}$.

In isotropic helical Saffman turbulence, $\mathcal{E}_0(\tilde{\boldsymbol{k}})$ and $\mathcal{H}_0(\tilde{\boldsymbol{k}})$ must be $\tilde{\boldsymbol{k}}$ independent and $\mathcal{Z}_0(\tilde{\boldsymbol{k}}) = 0$. Equations (17) and (18) may be reduced to

$$\hat{R}_{ij}(\boldsymbol{k}) = \mathcal{E}_0^{(I)} P_{ij} + i\mathcal{H}_0^{(I)} \epsilon_{ij\alpha} \tilde{k}_\alpha + o(1), \tag{19}$$

$$\hat{R}_{ij}^{\pm}(\boldsymbol{k}) = \tfrac{1}{2}\big(\mathcal{E}_0^{(I)} \pm \mathcal{H}_0^{(I)}\big) N_i(-\tilde{\boldsymbol{k}}) N_j(\tilde{\boldsymbol{k}}) + o(1), \tag{20}$$

where $\mathcal{E}_0^{(I)}$ and $\mathcal{H}_0^{(I)}$ are $\tilde{\boldsymbol{k}}$-independent constants. Generally, Eq. (18) implies that $\langle \boldsymbol{u}^{\pm}(\boldsymbol{x}) \cdot \boldsymbol{u}^{\pm}(\boldsymbol{x} + \boldsymbol{r})\rangle = O(r^{-3})$ at $r \to \infty$. For isotropic helical Saffman turbulence with Eq. (20), $\langle \boldsymbol{u}^{\pm}(\boldsymbol{x}) \cdot \boldsymbol{u}^{\pm}(\boldsymbol{x} + \boldsymbol{r})\rangle = o(r^{-3})$ at $r \to \infty$.

For incompressible homogeneous turbulence obeying the Navier-Stokes equation (4), it was shown in Ref. [3] that

$$\frac{\partial}{\partial t} \hat{R}_{ij}(\boldsymbol{k}, t) = O(k) \quad \text{for any } t \geqslant t_0, \tag{21}$$

so that the $O(k^0)$ term in Eq. (17) is time independent for any t ($\geqslant t_0$). Then we obtain that

$$\mathcal{E}_0(\tilde{\boldsymbol{k}}),\ \mathcal{H}_0(\tilde{\boldsymbol{k}}),\ \mathcal{Z}_0(\tilde{\boldsymbol{k}}) \text{ are time independent.} \tag{22}$$

Equations (8), (10), and (22) mean that the energy spectrum $E(k)$ and helicity spectrum $H(k)$ have the form

$$E(k) = Ck^2 + o(k^2), \quad H(k) = C_h k^3 + o(k^3) \quad \text{at } k \to 0, \tag{23}$$

where C (>0) and C_h are dynamical invariants. The $O(k^2)$ term in $E(k)$ and the $O(k^3)$ term in $H(k)$ are time independent.

C. Self-similarity

In Ref. [3] it was assumed that the velocity correlation spectral tensor $\hat{R}_{ij}(\boldsymbol{k}, t)$ for any i and j evolves at large scales including the energy containing range scales in accordance with the self-similar form

$$\hat{R}_{ij}(\boldsymbol{k}, t) = c_{ij}(t) f_{ij}(k_1\ell_1, k_2\ell_2, k_3\ell_3) = c_{ij}(t) f_{ij}(\boldsymbol{\zeta}) \tag{24}$$

in a certain "appropriate" time range and domain of the wave-vector space $\boldsymbol{k}$ including a small enough k range, where $\boldsymbol{\zeta}$ is a self-similar variable defined as $\boldsymbol{\zeta} = (k_1\ell_1, k_2\ell_2, k_3\ell_3)$, $c_{ij}(t)$ is independent of $\boldsymbol{k}$, $f_{ij}(\boldsymbol{\zeta})$ is a dimensionless function, and $\ell_m(t)$ is a length scale in the mth Cartesian direction. The time dependence of $\ell_m(t)$ was also assumed to be independent of components i and j of $\hat{R}_{ij}(\boldsymbol{k})$. A detailed description of appropriate in the large-scale self-similarity assumption (24) is given in the paragraph following Eq. (43). Then a simple analysis, which is based on the assumption (24) and the invariance of $\hat{R}_{ij}(\boldsymbol{k}, t)$ at $\boldsymbol{k} \to \boldsymbol{0}$, showed that

$$c_{ij} = \text{const}, \tag{25}$$

$$\frac{\ell_j}{\ell_i} = \text{const}, \tag{26}$$

and

$$\frac{\langle u_j^2 \rangle}{\langle u_i^2 \rangle} \simeq \text{const} \tag{27}$$

for any i and j [3]. Equations (26) and (27) imply the persistence of large-scale anisotropy in fully developed states and we can thus set $\ell_m = d_m \ell$, which implies that $\boldsymbol{\zeta}$ can be taken as

$$\boldsymbol{\zeta} = \boldsymbol{k}\ell, \tag{28}$$

where d_m is time independent and ℓ is an appropriate length scale.

Equation (15) implies that $\hat{R}_{ij}(\boldsymbol{k})$ is completely determined by the three scalars $\mathcal{E}(\boldsymbol{k})$, $\mathcal{Z}(\boldsymbol{k})$, and $\mathcal{H}(\boldsymbol{k})$: $\mathcal{E}(\boldsymbol{k}) = \frac{1}{2}\hat{R}_{\alpha\alpha}(\boldsymbol{k})$, $\mathcal{Z}(\boldsymbol{k}) = \frac{1}{2}\hat{R}_{\alpha\beta}(\boldsymbol{k})N_\alpha(-\tilde{\boldsymbol{k}})N_\beta(-\tilde{\boldsymbol{k}})$, and $\mathcal{H}(\boldsymbol{k}) = -\frac{i}{2}\tilde{k}_\alpha\epsilon_{\alpha\beta\gamma}\hat{R}_{\beta\gamma}(\boldsymbol{k})$ (e.g., Ref. [21]). In order to make the role of $\mathcal{H}(\boldsymbol{k}, t)$ transparent, we may rewrite Eq. (24) as

$$\mathcal{S}(\boldsymbol{k}, t) = c^{\mathcal{S}} f^{\mathcal{S}}(\boldsymbol{\zeta}), \tag{29}$$

where $\mathcal{S} = \mathcal{E}$, $\mathcal{Z}$, or $\mathcal{H}$; $c^{\mathcal{S}}$ is time independent because of Eq. (25); and $f^{\mathcal{S}}(\boldsymbol{\zeta})$ is a dimensionless function. These scalars evolve in accordance with the self-similar form (29) in the same time range and the $\boldsymbol{k}$ domain as the range and the domain where Eq. (24) holds. Without loss of generality, we may assume that $f^{\mathcal{S}}$ is normalized such that

$$\int_{\mathbb{R}^3} f^{\mathcal{S}}(\boldsymbol{\zeta}) d\boldsymbol{\zeta} = 1, \tag{30}$$

provided the integral of $f^{\mathcal{S}}$ over the entire domain of $\boldsymbol{k}$ is nonzero and finite. The time-independent constant $c^{\mathcal{S}}$ must have the dimensions (velocity)$^2 \times$ (length)^3. Equation (29) implies that the spectrum $\mathcal{S}(\boldsymbol{k}, t)$ depends on time t only through $\ell(t)$. By definition, the function $f^{\mathcal{S}}(\boldsymbol{\zeta})$ is time independent at any fixed $\boldsymbol{\zeta}$.

Consider the characteristic quantity associated with the field $\mathcal{S}(\boldsymbol{k}, t)$, which has the dimension (velocity)^2 and is defined by

$$\int_{\mathbb{R}^3} \mathcal{S}(\boldsymbol{k}) d\boldsymbol{k}. \tag{31}$$

By substituting Eq. (29) into the integral (31) and using Eqs. (28) and (30), we obtain

$$\int_{\mathbb{R}^3} c^{\mathcal{S}} f^{\mathcal{S}}(\boldsymbol{\zeta}) d\boldsymbol{k} = \frac{c^{\mathcal{S}}}{\ell^3} \int_{\mathbb{R}^3} f^{\mathcal{S}}(\boldsymbol{\zeta}) d\boldsymbol{\zeta} = \frac{c^{\mathcal{S}}}{\ell^3}. \tag{32}$$

Since $c^{\mathcal{S}}$ is time independent, Eq. (32) means

$$\int_{\mathbb{R}^3} \mathcal{S}(\boldsymbol{k}) d\boldsymbol{k}\, \ell^3 \simeq \text{const}. \tag{33}$$

As regards $\langle|\boldsymbol{u}|^2\rangle$ and $\langle|\boldsymbol{u}^+|^2\rangle - \langle|\boldsymbol{u}^-|^2\rangle$, Eqs. (11) and (32) give

$$\langle|\boldsymbol{u}|^2\rangle \ell^3 \simeq c^{\mathcal{E}}, \quad (\langle|\boldsymbol{u}^+|^2\rangle - \langle|\boldsymbol{u}^-|^2\rangle)\ell^3 \simeq c^{\mathcal{H}}. \tag{34}$$

Since $c^{\mathcal{E}}$ and $c^{\mathcal{H}}$ are time independent, Eq. (34) gives

$$\langle|\boldsymbol{u}|^2\rangle \ell^3 \simeq \text{const}, \quad (\langle|\boldsymbol{u}^+|^2\rangle - \langle|\boldsymbol{u}^-|^2\rangle)\ell^3 \simeq \text{const}, \tag{35}$$

from which we obtain

$$\langle|\boldsymbol{u}^\pm|^2\rangle \ell^3 \simeq \text{const}. \tag{36}$$

The time-independent values of Eqs. (35) and (36) may depend on $\langle|\boldsymbol{u}^\pm|^2\rangle$. Equation (35) implies the time independence of the degree of reflection asymmetry, i.e.,

$$\frac{\langle|\boldsymbol{u}^+|^2\rangle - \langle|\boldsymbol{u}^-|^2\rangle}{\langle|\boldsymbol{u}|^2\rangle} \simeq \text{const}. \tag{37}$$

Because of Eqs. (17), (24), (28), and (29),

$$c^{\mathcal{S}} f^{\mathcal{S}}(\boldsymbol{\zeta}) = c^{\mathcal{S}} f_0^{\mathcal{S}}(\boldsymbol{\zeta}/|\boldsymbol{\zeta}|) + o(1) \tag{38}$$

as $\boldsymbol{k} \to \boldsymbol{0}$, or equivalently $\boldsymbol{\zeta} \to \boldsymbol{0}$, where $f_0^{\mathcal{S}}$ may depend on the direction $\boldsymbol{\zeta}/|\boldsymbol{\zeta}|$ of $\boldsymbol{\zeta}$ but is independent of the magnitude $|\boldsymbol{\zeta}|$. Equation (22) implies the invariance of $\hat{R}_{ij}(\boldsymbol{k})$ at $\boldsymbol{k} \to \boldsymbol{0}$ for $t \geqslant t_0$. The time independence of $c^{\mathcal{H}}$ in the self-similar states and the invariance $\mathcal{H}_0(\tilde{\boldsymbol{k}})$ imply that if $\mathcal{H}_0(\tilde{\boldsymbol{k}}) \neq 0$ at an initial time instant $t = t_0$, then $c^{\mathcal{H}} \neq 0$ at any t in the self-similar states because of Eqs. (29) and (38). Hence, Eqs. (34) and (37) mean the persistence of the reflection asymmetry at the

large scales including the energy containing range scales, i.e., no return to reflection symmetry at the large scales for any anisotropic helical Saffman turbulence, if the large-scale structure is reflection asymmetric at $t = t_0$.

One might think that this large-scale persistence leads to the persistence of small-scale reflection asymmetry for homogeneous turbulence even at sufficiently high Reynolds number. However, this is not the case. The DNS [12] and the numerical simulation [13] showed that reflection symmetry is recovered at small scales, even if there is reflection asymmetry in the energy containing range owing to the injection of helicity.

The total helicity $\langle \boldsymbol{u} \cdot \boldsymbol{\omega} \rangle/2$ is given by the substitution of Eqs. (28) and (29) into Eq. (12):

$$\frac{1}{2}\langle \boldsymbol{u} \cdot \boldsymbol{\omega} \rangle \simeq c^{\mathcal{H}} \int_{\mathbb{R}^3} k f^{\mathcal{H}}(\boldsymbol{\zeta}) d\boldsymbol{k} = \frac{c^{\mathcal{H}}}{\ell^4} \int_{\mathbb{R}^3} |\boldsymbol{\zeta}| f^{\mathcal{H}}(\boldsymbol{\zeta}) d\boldsymbol{\zeta}. \tag{39}$$

Since $c^{\mathcal{H}}$ and $f^{\mathcal{H}}(\boldsymbol{\zeta})$ are time independent, this means that

$$\langle \boldsymbol{u} \cdot \boldsymbol{\omega} \rangle \ell^4 \simeq \text{const.} \tag{40}$$

Equations (35) and (40) show that

$$\frac{\langle \boldsymbol{u} \cdot \boldsymbol{\omega} \rangle \ell}{\langle |\boldsymbol{u}|^2 \rangle} \simeq \text{const.} \tag{41}$$

This ratio $\langle \boldsymbol{u} \cdot \boldsymbol{\omega} \rangle \ell / \langle |\boldsymbol{u}|^2 \rangle$ could be a quantity to measure the degree of reflection asymmetry of helical turbulent flows. However, the ratio is not so appropriate to estimate the degree, because the maximum value of $|\langle \boldsymbol{u} \cdot \boldsymbol{\omega} \rangle| \ell / \langle |\boldsymbol{u}|^2 \rangle$ depends on flow conditions such as the Reynolds number. The value cannot be determined *a priori*, in contrast to (13), whose maximum value is unity, as seen in the inequality (14).

For the comparison of the theory with experiments, it is convenient to introduce the integral length scale L_j defined as

$$L_j = \frac{\int_0^\infty \langle u_j(\boldsymbol{x}, t) u_j(\boldsymbol{x} + r\boldsymbol{i}_j, t) \rangle dr}{\langle u_j(\boldsymbol{x}, t)^2 \rangle}, \tag{42}$$

where the summation convention is not applied to the repeated roman subscripts. After simple algebra, it is shown that Eqs. (24) and (28) give

$$L_j \simeq \text{const} \times \ell. \tag{43}$$

It should be noted that we do not assume that the self-similar forms (24) and (29) are applicable to the entire time range and wave-vector domain. In fact, it is unlikely that they hold in premature states of turbulence or in the wave-vector domain of small scales in turbulence, e.g., the inertial subrange and the dissipation range. What is assumed in the derivation of Eqs. (34), (39), and (43) from Eqs. (11), (12), and (42), respectively, is that the integrals in Eqs. (11), (12), and (42) are dominated by the contributions from the wave-vector domain where $\mathcal{S}(\boldsymbol{k}, t)$ is well approximated by the self-similar form (29) in a certain time range of a mature or fully developed turbulence state. In the derivation of the time independence of c_{ij}, it is assumed that the wave-vector domain includes a sufficiently small k range. The time range and wave-vector domain are referred to as appropriate in the paragraph including Eq. (24).

D. Decay of energy and helicity

One may consider the decay rates of energy and helicity for anisotropic helical Saffman turbulence by a straightforward generalization of the discussion in Ref. [3]. Because of Eqs. (26) and (27), it is sufficient to consider one typical velocity v and one typical integral length scale L. We assume that the flux of energy to small scales is controlled by the energy containing eddies where the self-similar form (29) is a good approximation. It is then natural to assume that the decay rate

of $\langle|\boldsymbol{u}^{\pm}|^2\rangle$ may be expressed, as a first step approximation, by an appropriate functional of $\hat{R}_{ij}(\boldsymbol{k},t)$, or equivalently by $\mathcal{S}(\boldsymbol{k},t)$, so that

$$\frac{1}{2}\frac{d}{dt}\langle|\boldsymbol{u}|^2\rangle = -A^{\mathcal{E}}\frac{v^3}{L}, \quad \frac{1}{2}\frac{d}{dt}(\langle|\boldsymbol{u}^+|^2\rangle - \langle|\boldsymbol{u}^-|^2\rangle) = -A^{\mathcal{H}}\frac{v^3}{L}, \tag{44}$$

where $A^{\mathcal{S}}$ is an appropriate dimensionless functional of $\mathcal{S}$ and depends on ℓ. Here we can set $v^2 \propto \langle|\boldsymbol{u}|^2\rangle$.

Dimensional analysis and Eq. (29) suggest that the dimensionless coefficient A^S must be a functional of the dimensionless quantities $c^{\mathcal{S}}/v^2L^3$ and $f^{\mathcal{S}}$ in the fully developed states. Since $c^{\mathcal{S}}$, v^2L^3, and $f^{\mathcal{S}}$ are time independent as shown in Sec. II C, the coefficients $A^{\mathcal{E}}$ and $A^{\mathcal{H}}$ must be time independent. The integration of Eq. (44) under Eqs. (35) and (37) gives

$$\langle|\boldsymbol{u}|^2\rangle \propto t^{-6/5}, \tag{45}$$

$$L \propto t^{2/5}, \tag{46}$$

and

$$\langle|\boldsymbol{u}^+|^2\rangle - \langle|\boldsymbol{u}^-|^2\rangle \propto t^{-6/5} \tag{47}$$

at sufficiently large t. Equations (36), (40), and (46) give

$$\langle|\boldsymbol{u}^{\pm}|^2\rangle \propto t^{-6/5}, \tag{48}$$

$$\langle\boldsymbol{u}\cdot\boldsymbol{\omega}\rangle \propto t^{-8/5}. \tag{49}$$

The laws (45) and (46) are in accordance with Saffman's prediction [2] and are insensitive to the presence of helicity. This insensitivity may be expected from the independence of $\hat{R}_{\beta\beta}(\boldsymbol{k})$ from $\mathcal{H}(\boldsymbol{k})$ at $\boldsymbol{k}\to\boldsymbol{0}$, which is obtained by the contraction of i and j in Eq. (15).

Briard and Gomez [17] considered incompressible homogeneous helical isotropic turbulence whose energy spectrum $E(k)$ and helicity spectrum $H(k)$ at $k\to 0$ are given, respectively, by $E(k) = Bk^{\sigma} + o(k^{\sigma})$ and $H(k) = B_H k^{\sigma+1} + o(k^{\sigma+1})$ for $1 \leqslant \sigma \leqslant 4$, where B and B_H are k-independent constants. They obtained the decay laws of the turbulence, using an EDQNM closure, dimensional analysis based on the analysis by Ref. [18], and the relation $\langle\boldsymbol{u}\cdot\boldsymbol{\omega}\rangle \sim \langle|\boldsymbol{u}|^2\rangle/L_H$, where L_H is a helical integral length scale. It was assumed that the kinetic integral length scale of isotropic turbulence and L_H decay similarly. For isotropic helical Saffman turbulence ($\sigma = 2$), the decay laws (45), (46), and (49) are the same as the laws they obtained, and the relation (41) is in accordance with the relation $\langle\boldsymbol{u}\cdot\boldsymbol{\omega}\rangle \sim \langle|\boldsymbol{u}|^2\rangle/L_H$.

III. DIRECT NUMERICAL SIMULATION

A. Numerical methods and DNS parameters

We performed DNS of freely decaying turbulence in a periodic cubic box of side length 2π. Here, in order to focus on the influence of the invariance $\mathcal{H}_0(\tilde{\boldsymbol{k}})$ on generalized Saffman turbulence, we confine ourselves to quasi-isotropic turbulence. The flows obey Eq. (4) and the divergence-free condition. A Fourier spectral method and a fourth-order Runge-Kutta method are used. The aliasing errors are removed by a phase shift method. The Fourier modes satisfying $k < \sqrt{2}n_g/3$ are retained, where n_g is the number of grid points in each direction of the Cartesian coordinates. We use quasi-isotropic initial random fields whose energy spectra are given by $E(k) \propto k^2\exp(-k^2/k_p^2)$ and $\langle|\boldsymbol{u}(\boldsymbol{x},0)|^2\rangle = 1$. Here k_p is a peak wave number and the initial time t_0 is set to 0. Helicity is introduced into a quasinonhelical and quasi-isotropic random field (the Appendix). The initial helicity spectra $H(k)$ are given by $H(k) \propto k^3\exp(-k^2/k_p^2)$. We here focus on DNSs with n_g^3 ($=1024^3$) grid points and $k_p = 40$ among the DNSs we performed. The kinematic viscosity

TABLE I. DNS statistics at the initial time $t = 0$.

Run	Re	$\langle \boldsymbol{u} \cdot \boldsymbol{\omega} \rangle / 2$	$\langle \boldsymbol{u} \cdot \boldsymbol{\omega} \rangle / \sqrt{\langle \lvert\boldsymbol{u}\rvert^2 \rangle \langle \lvert\boldsymbol{\omega}\rvert^2 \rangle}$
1	159	10.5	0.43
2	159	17.0	0.69
3	161	0.0	0.0

$\nu = 2.4 \times 10^{-4}$, the time increment is 6.25×10^{-4}, and the initial $k_{\max}\eta = 1.1$, where $k_{\max}$ is the maximum wave number and η is the Kolmogorov microscale. Table I presents other statistics at the initial time $t = 0$. Runs 1 and 2 represent the DNSs of helical turbulence, whereas run 3 represents the DNS of quasinonhelical turbulence as a reference. Figure 1 shows the evolution of the Reynolds number defined as $\mathrm{Re} = vL/\nu$, where v and L are given by

$$v = \sqrt{\frac{\langle |\boldsymbol{u}(\boldsymbol{x}, t)|^2 \rangle}{3}}, \quad L = \frac{L_1 + L_2 + L_3}{3}. \tag{50}$$

The time t is normalized by the initial large-eddy turnover time T, which is defined as $T = 1/k_p \langle |\boldsymbol{u}(\boldsymbol{x}, 0)|^2 \rangle^{1/2}$ and here $T = 1/k_p$. The Reynolds number in the DNSs is moderate but high enough so as to simulate fully developed freely decaying turbulence (see Ref. [4]). In the DNS with 1024^3 grid points and $k_p = 80$, which uses the same initial relative helicity as that of run 1, it was confirmed that the large-scale resolution of run 1 is sufficient to examine the decay of the helical Saffman turbulence (figure omitted).

B. DNS results

We examine whether the invariance and the decay laws in Sec. II hold well or not, using DNS. The flows in all runs become mature or fully developed after the early transient time period, i.e., for $t/T \gtrsim 60$ in run 1, $t/T \gtrsim 100$ in run 2, and $t/T \gtrsim 40$ in run 3 (DNS of the quasinonhelical flow). It can be seen in Figs. 2(a) and 2(b) that for fully developed helical turbulence, $\langle |\boldsymbol{u}|^2 \rangle / 2$ decays approximately as $t^{-6/5}$ and the length scale L grows approximately as $t^{2/5}$. Figures 2(c) and 2(d), which are replots of $\langle |\boldsymbol{u}|^2 \rangle / 2$ and L in compensated forms, show that $t^{6/5} \langle |\boldsymbol{u}|^2 \rangle / 2$ and $t^{-2/5} L$ are nearly time independent in the fully developed turbulence. This confirms that the power laws (45) and (46), i.e., $\langle |\boldsymbol{u}|^2 \rangle \propto t^{-6/5}$ and $L \propto t^{2/5}$, are good approximations to the evolution of $\langle |\boldsymbol{u}|^2 \rangle / 2$ and L in the fully developed states. Thus, the decay of $\langle |\boldsymbol{u}|^2 \rangle / 2$ and the growth of L are insensitive to the presence of helicity. It was confirmed that the flows in all runs remain quasi-isotropic in the sense that $\langle u_1^2 \rangle \approx \langle u_2^2 \rangle \approx \langle u_3^2 \rangle$ and $L_1 \approx L_2 \approx L_3$ (figure omitted). The results for run 3 are consistent

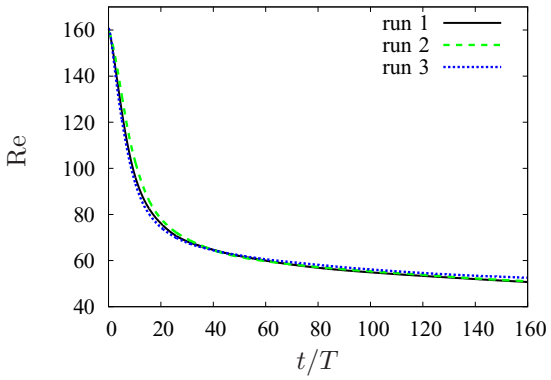

FIG. 1. Plot of Re with normalized time t/T.

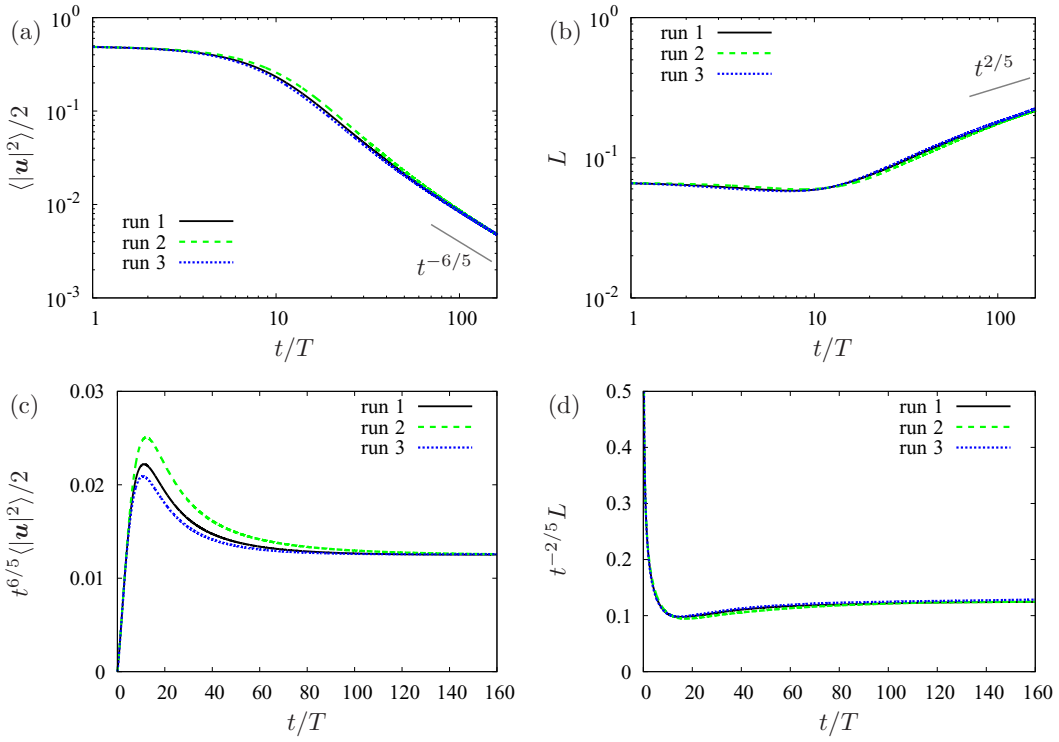

FIG. 2. Evolution of (a) kinetic energy $\langle|\boldsymbol{u}|^2\rangle/2$, (b) integral length scale L, (c) compensated kinetic energy $t^{6/5}\langle|\boldsymbol{u}|^2\rangle/2$, and (d) compensated integral length scale $t^{-2/5}L$.

with the DNS results [4] for quasi-isotropic nonhelical Saffman turbulence. The length of the early period of the premature states increases as the initial helicity (in Table I) becomes stronger. This agrees with the EDQNM prediction [14] and DNS results [25] showing that helicity slows down the development of small scales in the early period.

Figure 3 shows the evolution of $(\langle|\boldsymbol{u}^+|^2\rangle - \langle|\boldsymbol{u}^-|^2\rangle)/2$ for runs 1 and 2. It can be seen in Fig. 3(a) that $(\langle|\boldsymbol{u}^+|^2\rangle - \langle|\boldsymbol{u}^-|^2\rangle)/2$ decays approximately as $t^{-6/5}$ in the fully developed states. The power-law-like behavior is confirmed by the plots of the compensated form $t^{6/5}(\langle|\boldsymbol{u}^+|^2\rangle - \langle|\boldsymbol{u}^-|^2\rangle)/2$ in Fig. 3(b). For run 3, whose initial helicity is almost zero, $\langle|\boldsymbol{u}^+|^2\rangle - \langle|\boldsymbol{u}^-|^2\rangle \approx 0$, as

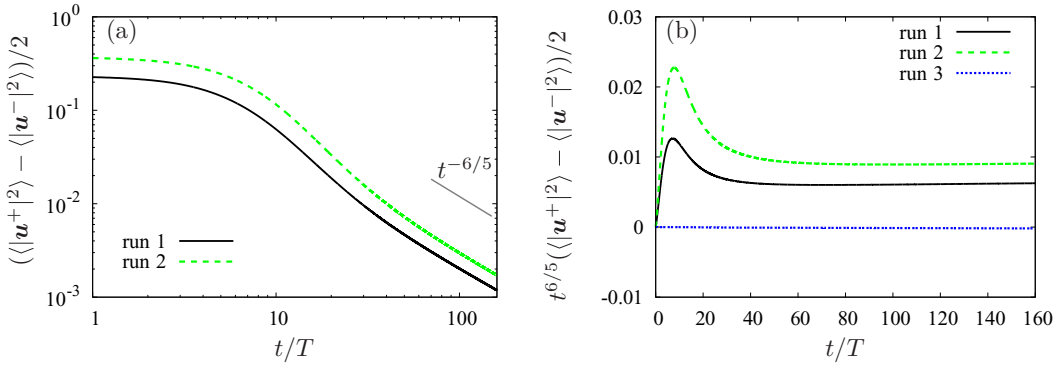

FIG. 3. Evolution of (a) $(\langle|\boldsymbol{u}^+|^2\rangle - \langle|\boldsymbol{u}^-|^2\rangle)/2$ and (b) $t^{6/5}(\langle|\boldsymbol{u}^+|^2\rangle - \langle|\boldsymbol{u}^-|^2\rangle)/2$.

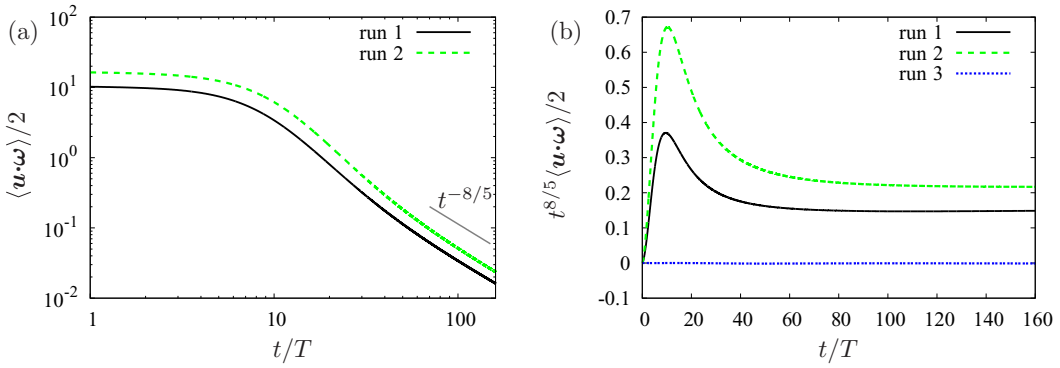

FIG. 4. Evolution of (a) helicity $\langle \boldsymbol{u}\cdot\boldsymbol{\omega}\rangle/2$ and (b) $t^{8/5}\langle \boldsymbol{u}\cdot\boldsymbol{\omega}\rangle/2$.

shown in Fig. 3(b). The flow in run 3 is quasinonhelical. Figure 4 shows that the helicity $\langle \boldsymbol{u}\cdot\boldsymbol{\omega}\rangle/2$ decays approximately as $t^{-8/5}$ in the fully developed states for runs 1 and 2. The compensated helicity $t^{8/5}\langle \boldsymbol{u}\cdot\boldsymbol{\omega}\rangle/2$ remains constant in these states. Therefore, the results shown in Figs. 3 and 4 support the decay laws (47) and (49). These results suggest that $\langle \boldsymbol{u}\cdot\boldsymbol{\omega}\rangle/2 \propto v^2/L$ and the timescale of the helicity decay is L/v, where v is defined by Eq. (50). It is shown in Fig. 4(b) that $\langle \boldsymbol{u}\cdot\boldsymbol{\omega}\rangle \approx 0$ for the quasinonhelical turbulence in run 3. Figure 5 shows the time developments of $A^{\mathcal{E}}$ and $A^{\mathcal{H}}$ in Eq. (44). After the time periods corresponding to the premature states, $A^{\mathcal{E}}$ and $A^{\mathcal{H}}$ are approximately constant in all runs. In Figs. 2–4 it can be seen that the evolution of $\langle|\boldsymbol{u}|^2\rangle$, L, $\langle|\boldsymbol{u}^{\pm}|^2\rangle$, and $\langle \boldsymbol{u}\cdot\boldsymbol{\omega}\rangle$ does not obey the decay laws in the strict sense. Hence $A^{\mathcal{E}}$ and $A^{\mathcal{H}}$ are not strictly constant as shown in Fig. 5. However, it should be noted that the decay laws are consistent with the DNS.

Figure 6 shows the evolution of the degree of reflection asymmetry (13) based on $\langle|\boldsymbol{u}^{\pm}|^2\rangle$, which are representative quantities in the energy containing range. For the fully developed turbulence, the value of the degree is nearly time independent in each run. In other words, Eq. (37) holds well. This means the persistence of reflection asymmetry in the energy containing range for runs 1 and 2. The degree in the fully developed states becomes stronger with the initial magnitude of the helicity. The value of the degree remains nearly zero for run 3. Thus, the flow in run 3 is quasireflection symmetric.

Figures 7(a) and 7(b) show, respectively, the time development of the spherically averaged energy spectra $E_{\mathrm{ave}}(k) = E(k)/4\pi k^2$ and normalized spherically averaged helicity spectra $H_{\mathrm{ave}}(k)/k = H(k)/4\pi k^3$ for run 1. At low wave numbers, these spectra remain nearly flat and are almost time independent. These observations at low wave numbers provide confirmation of the dynamical

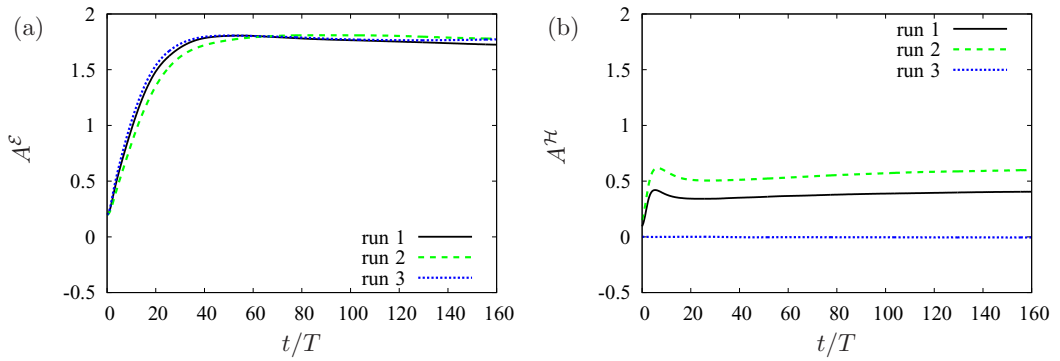

FIG. 5. Plot of $A^{\mathcal{E}}$ and $A^{\mathcal{H}}$ vs t/T.

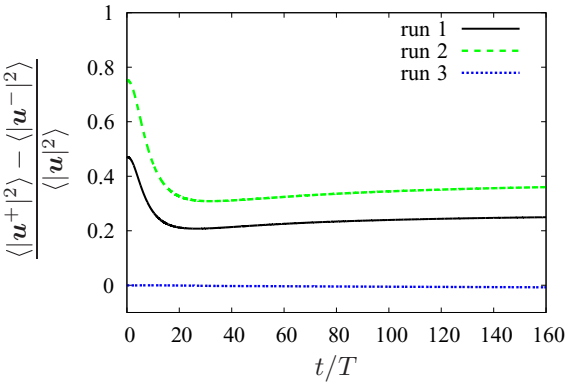

FIG. 6. Plot of $(\langle|\boldsymbol{u}^+|^2\rangle - \langle|\boldsymbol{u}^-|^2\rangle)/\langle|\boldsymbol{u}|^2\rangle$ vs t/T.

invariance of C and C_h in Eq. (23). Therefore, the turbulence in run 1 can be regarded as helical Saffman turbulence.

Figures 8(a) and 8(b) show, respectively, the kL dependence of normalized spectra $E_{\rm ave}(k)/v^2L^3$ and $H_{\rm ave}(k)/kv^2L^3$ for run 1 at different time instants. As suggested by Fig. 2, v^2L^3 is nearly constant in the fully developed states. It can be observed in Fig. 8(a) that the spectra $E_{\rm ave}(k)/v^2L^3$ in the fully developed state, i.e., for $t/T \gtrsim 60$, collapse well. This collapse shows the self-similarity of the fully developed turbulence at least approximately. Good collapse of $H_{\rm ave}(k)/kv^2L^3$ can also be seen in Fig. 8(b). The collapse suggests that the growth rate of ℓ is independent of the existence of nonzero $\mathcal{H}(\boldsymbol{k})$, which is consistent with the assumption in Eq. (24). The spectra $E(k)$ for runs 2 and 3 and also the helicity spectrum $H(k)$ for run 2 are omitted, because the results are similar to those presented here.

The normalized spectra look as if they collapse well in all wave-number ranges including the dissipation range. One might think that the velocity correlation spectral tensor $\hat{R}_{ij}(\boldsymbol{k}, t)$ is self-similar in the wave-number range and that all statistics are governed by L, v, and the timescale L/v. The large-scale self-similarity assumption is not imposed on small scales such as the dissipation range scales, as mentioned in Sec. II C. If $\hat{R}_{ij}(\boldsymbol{k}, t)$ was completely self-similar over the entire k range, then the enstrophy decay of the flow would be predicted as follows. If Eqs. (28) and (29) were applied to $\langle|\boldsymbol{\omega}|^2\rangle = \int_{\mathbb{R}^3} k^2|\hat{\boldsymbol{u}}(\boldsymbol{k})|^2 d\boldsymbol{k}$, then we had that $\langle|\boldsymbol{\omega}|^2\rangle\ell^5$ is time independent and $\langle|\boldsymbol{\omega}|^2\rangle/2 \propto t^{-2}$, because $\ell \propto L$ and $L \propto t^{2/5}$. However, this is not the case. Figure 9 shows

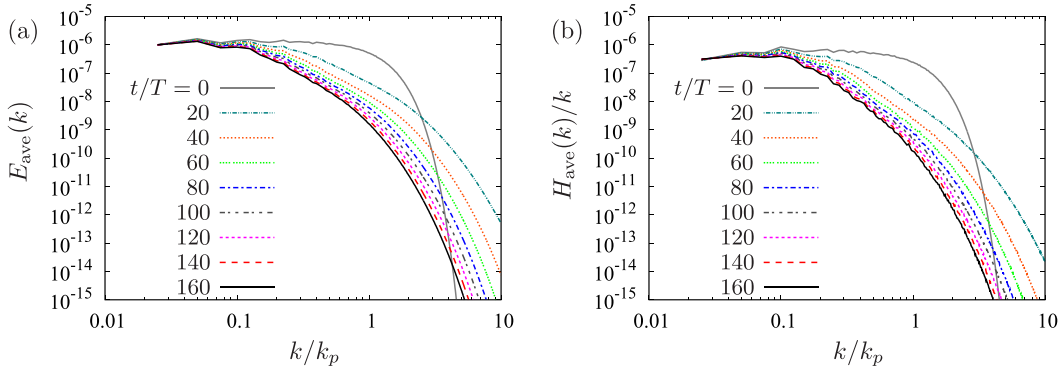

FIG. 7. Spectra for run 1 at $t/T = 0$, 20, 40, 60, 80, 100, 120, 140, and 160: (a) $E_{\rm ave}(k) = E(k)/4\pi k^2$ vs k/k_p and (b) $H_{\rm ave}(k)/k = H(k)/4\pi k^3$ vs k/k_p.

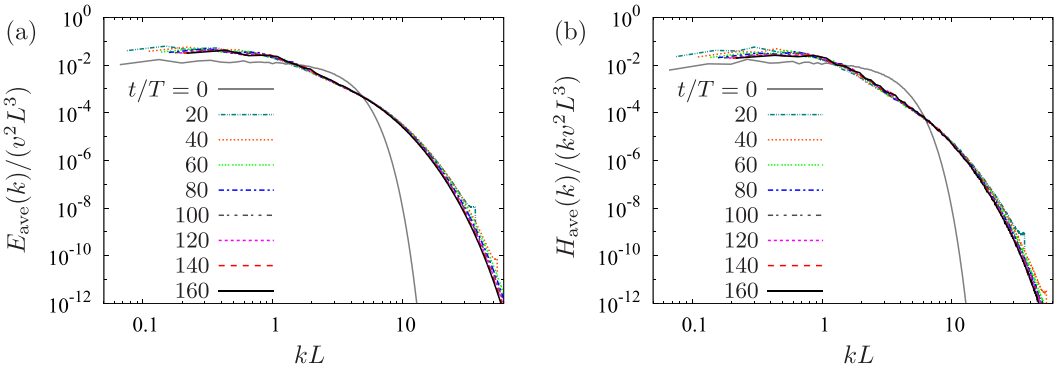

FIG. 8. Normalized spectra for run 1 at $t/T = 0$, 20, 40, 60, 80, 100, 120, 140, and 160: (a) $E_{\rm ave}(k)/v^2L^3$ vs kL and (b) $H_{\rm ave}(k)/kv^2L^3$ vs kL.

that the enstrophy decays approximately as t^{-2-s}, with s being approximately 0.3 in the DNSs. The enstrophy is dominated by contributions from the dissipation range. This is in accordance with Ref. [26], showing that complete self-similarity in the decay of incompressible homogeneous isotropic flow was found only for $E(k)$ given by $C_1k + o(k)$ at $k \to 0$, with C_1 being a k-independent constant. For runs 2 and 3, the enstrophy decays like $\langle|\boldsymbol{\omega}|^2\rangle/2 \propto t^{-2.3}$ in the fully developed states and thus we omitted these results in Fig. 9(b).

Figure 10 shows the time development of the relative helicity $\langle \boldsymbol{u}\cdot\boldsymbol{\omega}\rangle/\sqrt{\langle|\boldsymbol{u}|^2\rangle\langle|\boldsymbol{\omega}|^2\rangle}$, which also characterizes the degree of reflection asymmetry. It can be seen that for fully developed helical Saffman turbulence, the time dependence of the relative helicity is weak. The dependence is given by $\langle \boldsymbol{u}\cdot\boldsymbol{\omega}\rangle/\sqrt{\langle|\boldsymbol{u}|^2\rangle\langle|\boldsymbol{\omega}|^2\rangle} \propto t^{s/2}$ ($s \approx 0.3$), which is obtained by $\langle|\boldsymbol{u}|^2\rangle \propto t^{-6/5}$, $\langle \boldsymbol{u}\cdot\boldsymbol{\omega}\rangle \propto t^{-8/5}$, and $\langle|\boldsymbol{\omega}|^2\rangle \propto t^{-2.3}$. Therefore, the relative helicity is an appropriate alternative to the measure (13) showing the persistence of large-scale reflection asymmetry, as long as the exponent $s/2$ is sufficiently small in the fully developed states. In order to reduce the contribution from the dissipation range to the relative helicity, one may use low-pass filtering of velocity and vorticity fields. The relative filtered helicity can better represent the degree of large-scale reflection asymmetry than the relative helicity $\langle \boldsymbol{u}\cdot\boldsymbol{\omega}\rangle/\sqrt{\langle|\boldsymbol{u}|^2\rangle\langle|\boldsymbol{\omega}|^2\rangle}$.

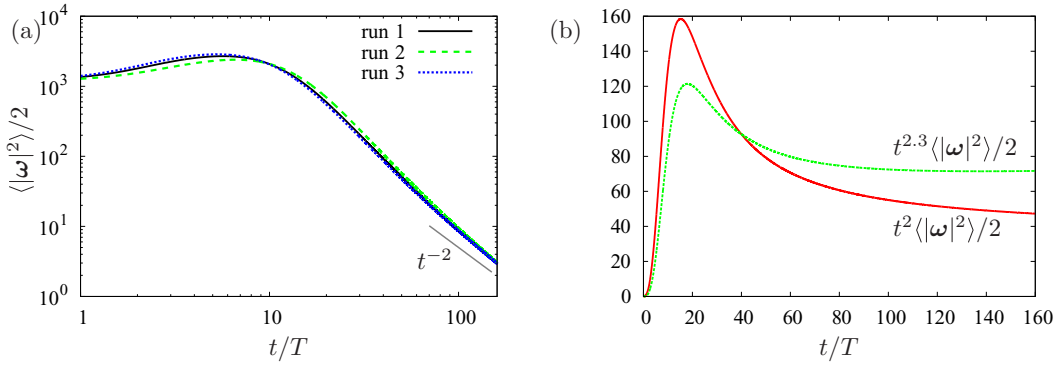

FIG. 9. (a) Enstrophy $\langle|\boldsymbol{\omega}|^2\rangle/2$ vs t/T for all runs and (b) $t^2\langle|\boldsymbol{\omega}|^2\rangle/2$ and $t^{2.3}\langle|\boldsymbol{\omega}|^2\rangle/2$ vs t/T for run 1.

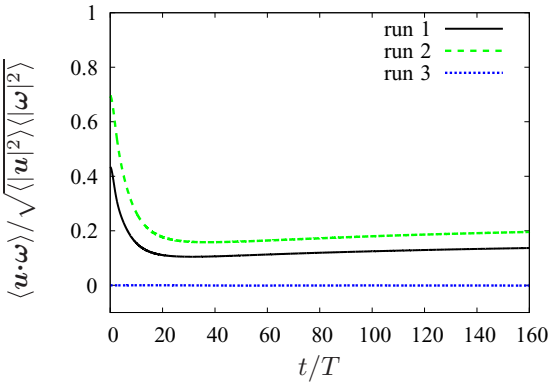

FIG. 10. Relative helicity $\langle \boldsymbol{u}\cdot\boldsymbol{\omega}\rangle/\sqrt{\langle|\boldsymbol{u}|^2\rangle\langle|\boldsymbol{\omega}|^2\rangle}$ vs t/T.

IV. CONCLUSION

We considered the large-scale structure of freely decaying incompressible homogeneous anisotropic turbulence in the presence of helicity, in which the energy spectrum $E(k)$ and the helicity spectrum $H(k)$ are given by $E(k) = Ck^2 + o(k^2)$ and $H(k) = C_h k^3 + o(k^3)$, respectively, at $k \to 0$. Here C and C_h are k independent and C is a dynamical invariant. Saffman's argument [1] for nonhelical turbulence was generalized to helical turbulence. The generalized turbulence is called here helical Saffman turbulence. Generally, the leading $O(k^0)$ term of the velocity correlation spectral tensor $\hat{R}_{ij}(\boldsymbol{k})$ at $\boldsymbol{k} \to \boldsymbol{0}$ is reflection asymmetric and time independent. Following Ref. [3], we showed that C_h is another dynamical invariant.

The measure characterizing the degree of reflection asymmetry at the large scales including the energy containing range scales was introduced by the use of $\boldsymbol{u}^+(\boldsymbol{x})$ and $\boldsymbol{u}^-(\boldsymbol{x})$ whose Fourier transforms $\hat{\boldsymbol{u}}^+(\boldsymbol{k})$ and $\hat{\boldsymbol{u}}^-(\boldsymbol{k})$ have non-negative and nonpositive helicity, respectively. These two fields are obtained by the helical decomposition of $\hat{\boldsymbol{u}}(\boldsymbol{k})$. A theoretical analysis based on the invariance of the $O(k^0)$ term of $\hat{R}_{ij}(\boldsymbol{k})$ at $\boldsymbol{k} \to \boldsymbol{0}$ and the self-similarity assumption of the large-scale evolution shows the persistence of the large-scale reflection asymmetry for fully developed anisotropic helical Saffman turbulence if the $O(k^0)$ term is reflection asymmetric at an initial instant. This persistence means no return to reflection symmetry at the large scales. Dimensional analysis then yields the decay laws for fully developed anisotropic helical Saffman turbulence.

We performed DNSs of incompressible turbulence in a periodic box with 1024^3 grid points, using a Fourier spectral method. It was shown that the self-similarity holds well for the fully developed states. The DNS results are in accordance with the theoretical results at least approximately. Strictly speaking, the DNS results show a small departure from the decay laws. It can also be seen in Fig. 7 that the spectra $E_{\rm ave}(k)$ and $H_{\rm ave}(k)/k$ at low wave numbers are not strictly time independent. The small discrepancy from the theoretical results may be due to the influence of Re, the box size, small-scale resolution $k_{\max}\eta$, and the number of the realizations in taking the ensemble average of the DNS results. Direct numerical simulation is free from any error arising from turbulent modeling or closure assumptions. Therefore, a DNS convergence study about the influence might be interesting. However, this is beyond the scope of this work. Such a DNS study would have a very high computational cost.

ACKNOWLEDGMENTS

The computations were carried out on the FX100 systems at the Information Technology Center of Nagoya University. The authors thank Professor N. Okamoto for making the code used in Ref. [4] available at the FX100. This work was supported by Grants-in-Aid for Scientific Research, No.

(S)16H06339 and No. (C)17K05573, from the Japan Society for the Promotion of Science. The authors acknowledge International Academic Network supported by the Leverhulme Trust "Waves and turbulence in rotating, stratified and electrically conducting fluids."

APPENDIX: IINITIAL VELOCITY FIELDS WITH HELICITY

In our DNS, the initial velocity fields were generated as $\hat{\boldsymbol{u}}(\boldsymbol{k},0) = G(k)\{\boldsymbol{a}^i(\boldsymbol{k}) + \Lambda \boldsymbol{a}^h(\boldsymbol{k})\}$, where $G(k) \propto k^2 \exp(-k^2/k_p^2)$, $\langle|\boldsymbol{u}(\boldsymbol{x},0)|^2\rangle = 1$, and Λ is real. For the helical flows in runs 1 and 2, $\Lambda = 4$, while $\Lambda = 0$ for the nonhelical flow in run 3. Both fields $\boldsymbol{a}^i(\boldsymbol{k})$ and $\boldsymbol{a}^h(\boldsymbol{k})$ are solenoidal and statistically isotropic. The field $\boldsymbol{a}^i(\boldsymbol{k})$ has statistically reflection symmetry, whereas, as described in the next paragraph, $\boldsymbol{a}^h(\boldsymbol{k})$ has statistically antireflection symmetry owing to the helicity. [A field of the form $\boldsymbol{b}(\boldsymbol{k}) \times i\boldsymbol{k}/k$ was used as the initial field in run 13 of Ref. [4]. However, $\boldsymbol{b}(\boldsymbol{k})$ is a nonhelical velocity field in Ref. [4] and thus $\boldsymbol{b}(\boldsymbol{k}) \times i\boldsymbol{k}/k$ is nonhelical.]

The solenoidal field $\boldsymbol{a}^\kappa(\boldsymbol{k})$ is written as $\boldsymbol{a}^\kappa(\boldsymbol{k}) = \phi_1^\kappa(\boldsymbol{k})\boldsymbol{e}^{(1)}(\boldsymbol{k}) + \phi_2^\kappa(\boldsymbol{k})\boldsymbol{e}^{(2)}(\boldsymbol{k})$ ($\kappa = i, h$), by the use of the Craya-Herring decomposition. Here $\{\phi_1^\kappa(\boldsymbol{k})\}^* = -\phi_1^\kappa(-\boldsymbol{k})$, $\{\phi_2^\kappa(\boldsymbol{k})\}^* = \phi_2^\kappa(-\boldsymbol{k})$, and $\langle|\phi_1^\kappa(\boldsymbol{k})|^2\rangle = \langle|\phi_2^\kappa(\boldsymbol{k})|^2\rangle$. The complex functions $\phi_1^\kappa(\boldsymbol{k})$ and $\phi_2^\kappa(\boldsymbol{k})$ are produced by eight sets of real normal random numbers $X_j(\boldsymbol{k})$ ($j = 1, 2, \ldots, 8$) satisfying $\langle X_j(\boldsymbol{k})\rangle = 0$ and $\langle X_j(\boldsymbol{k})X_l(\boldsymbol{k})\rangle = \delta_{jl}$. For the field $\boldsymbol{a}^h(\boldsymbol{k})$ with helicity, we set $\phi_1^h(\boldsymbol{k}) = X_1(\boldsymbol{k}) + iX_2(\boldsymbol{k})$ and $\phi_2^h(\boldsymbol{k}) = Y_1(\boldsymbol{k}) + iY_2(\boldsymbol{k})$. Here $Y_j(\boldsymbol{k})$ ($j = 1, 2$) are defined by

$$Y_1(\boldsymbol{k}) = -\lambda X_2(\boldsymbol{k}) + \sqrt{1-\lambda^2}X_3(\boldsymbol{k}), \tag{A1}$$

$$Y_2(\boldsymbol{k}) = \lambda X_1(\boldsymbol{k}) + \sqrt{1-\lambda^2}X_4(\boldsymbol{k}), \tag{A2}$$

where λ is a constant satisfying $|\lambda| \leqslant 1$, $\langle X_2(\boldsymbol{k})Y_1(\boldsymbol{k})\rangle = -\lambda$, and $\langle X_1(\boldsymbol{k})Y_2(\boldsymbol{k})\rangle = \lambda$. Since $\langle\{\phi_1^h(\boldsymbol{k})\}^*\phi_2^h(\boldsymbol{k})\rangle = 2i\lambda$, we have $\mathcal{H}(\boldsymbol{k}) = 2\lambda$. We set $\lambda = 0.5$ for run 1 and $\lambda = 0.8$ for run 2. For the field $\boldsymbol{a}^i(\boldsymbol{k})$ with reflection symmetry, we set $\phi_1^i(\boldsymbol{k}) = X_5(\boldsymbol{k}) + iX_6(\boldsymbol{k})$ and $\phi_2^i(\boldsymbol{k}) = X_7(\boldsymbol{k}) + iX_8(\boldsymbol{k})$.

[1] P. G. Saffman, The large-scale structure of homogeneous turbulence, J. Fluid Mech. **27**, 581 (1967).
[2] P. G. Saffman, Note on decay of homogeneous turbulence, Phys. Fluids **10**, 1349 (1967).
[3] K. Yoshimatsu and Y. Kaneda, Large-scale structure of velocity and passive scalar fields in freely decaying homogeneous anisotropic turbulence, Phys. Rev. Fluids **3**, 104601 (2018).
[4] P. A. Davidson, N. Okamoto, and Y. Kaneda, On freely decaying, anisotropic, axisymmetric Saffman turbulence, J. Fluid Mech. **706**, 150 (2012).
[5] J. R. Chasnov, The decay of axisymmetric homogeneous turbulence, Phys. Fluids **7**, 600 (1995).
[6] V. Mons, M. Meldi, and P. Sagaut, Numerical investigation on the partial return to isotropy of freely decaying homogeneous axisymmetric turbulence, Phys. Fluids **26**, 025110 (2014).
[7] V. Mons, C. Cambon, and P. Sagaut, A spectral model for homogeneous shear-driven anisotropic turbulence in terms of spherically averaged descriptors, J. Fluid Mech. **788**, 147 (2016).
[8] H. K. Moffatt and A. Tsinober, Helicity in laminar and turbulent flow, Annu. Rev. Fluid Mech. **24**, 281 (1992).
[9] H. K. Moffatt, Helicity and singular structures in fluid dynamics, Proc. Natl. Acad. Sci. USA **111**, 3663 (2014).
[10] E. Kit, A. Tsinober, J. L. Balint, J. M. Wallace, and E. Levich, An experimental study of helicity related properties of a turbulent flow past a grid, Phys. Fluids **30**, 3323 (1987).
[11] Q. Chen, S. Chen, G. L. Eyink, and D. D. Holm, Intermittency in the Joint Cascade of Energy and Helicity, Phys. Rev. Lett. **90**, 214503 (2003).
[12] S. Kurien, M. A. Taylor, and T. Matsumoto, Cascade time scales for energy and helicity in homogeneous isotropic turbulence, Phys. Rev. E **69**, 066313 (2004).

[13] V. Borue and S. A. Orszag, Spectra in helical three-dimensional homogeneous isotropic turbulence, Phys. Rev. E **55**, 7005 (1997).
[14] J. C. André and M. Lesieur, Influence of helicity on the evolution of isotropic turbulence at high Reynolds number, J. Fluid Mech. **81**, 187 (1977).
[15] A. Brissaud, U. Frisch, J. Leorat, M. Lesieur, and A. Mazure, Helicity cascade in fully developed isotropic turbulence, Phys. Fluids **16**, 1366 (1973).
[16] R. H. Kraichnan, Helical turbulence and absolute equilibrium, J. Fluid Mech. **59**, 745 (1973).
[17] A. Briard and T. Gomez, Dynamics of helicity in homogeneous skew-isotropic turbulence, J. Fluid Mech. **821**, 539 (2017).
[18] G. Comte-Bellot and S. Corrsin, The use of a contraction to improve the isotropy of grid-generated turbulence, J. Fluid Mech **25**, 657 (1966).
[19] A. O. Levshin and O. G. Chkhetiani, Decay of helicity in homogeneous turbulence, JETP Lett. **98**, 598 (2013).
[20] C. Cambon and L. Jacquin, Spectral approach to non-isotropic turbulence subjected to rotation, J. Fluid Mech. **202**, 295 (1989).
[21] P. Sagaut and C. Cambon, *Homogeneous Turbulence Dynamics*, 2nd ed. (Springer International, Cham, 2018).
[22] R. Betchov, Semi-isotropic turbulence and helicoidal flows, Phys. Fluids **4**, 925 (1961).
[23] Q. Chen, S. Chen, and G. L. Eyink, The joint cascade of energy and helicity in three-dimensional turbulence, Phys. Fluids **15**, 361 (2003).
[24] A. Alexakis, Helically decomposed turbulence, J. Fluid Mech. **812**, 752 (2017).
[25] W. Polifke and L. Shtilman, The dynamics of helical decaying turbulence, Phys. Fluids A **1**, 2025 (1989).
[26] M. Meldi and P. Sagaut, Further insights into self-similarity and self-preservation in freely decaying isotropic turbulence, J. Turbul. **14**, 24 (2013).